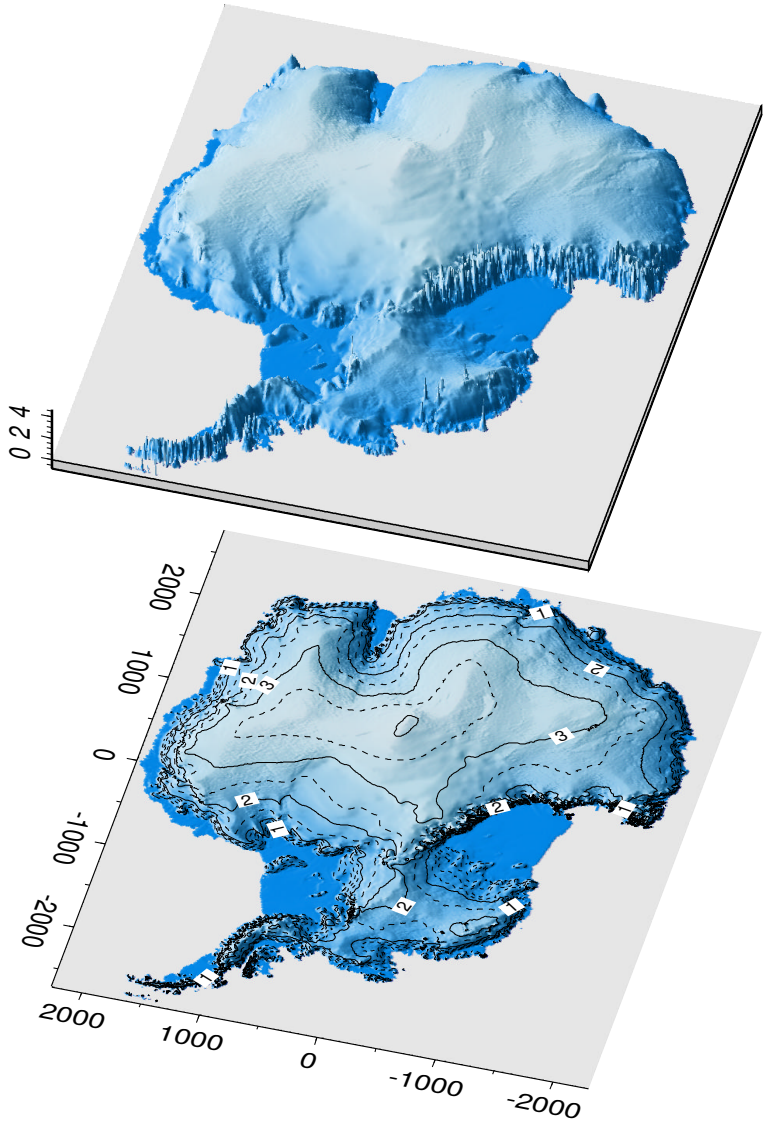

Figure II.28.: The *Radarsat Antarctic Mapping Project Digital Elevation Model* (RAMP-DEM), Liu et al. (2000). Isolines: 1 km solid, 0.5 km dashed.

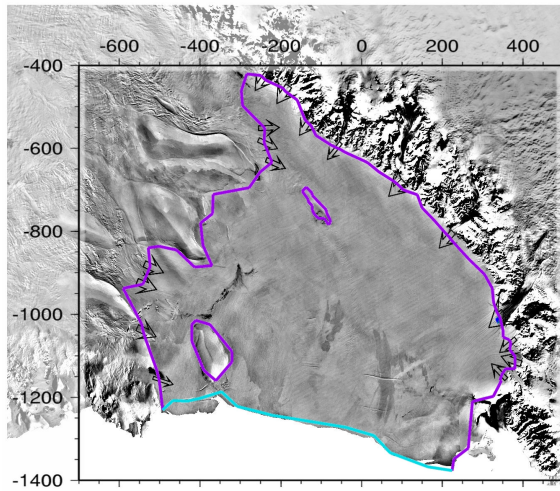

(a) Grounding-line position mapped onto an AVHRR satellite image.

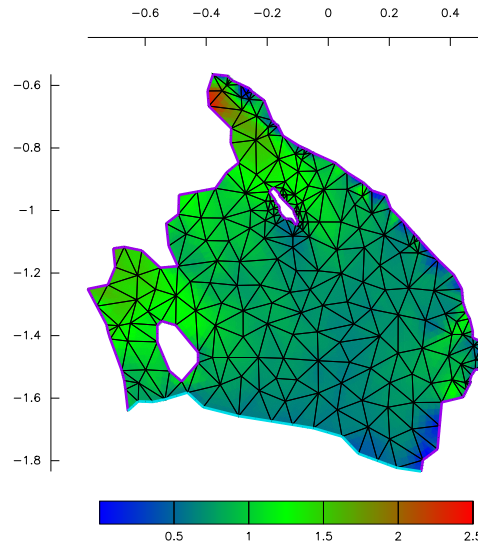

(b) Ice thickness of the FE dataset.

Figure II.29.: Data sets used for the computation for the Ross Ice Shelf.

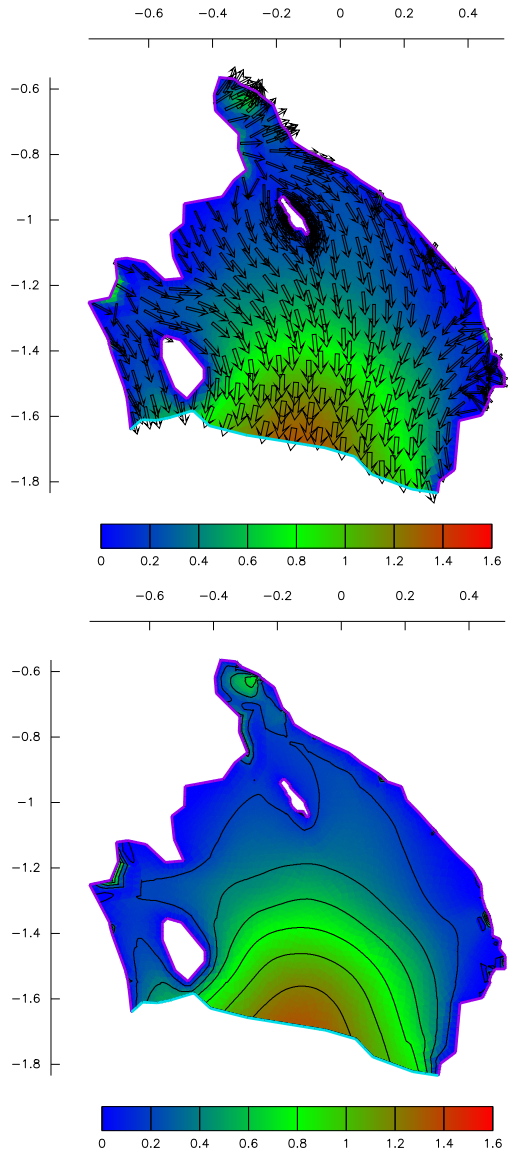

Figure II.30.: Computed velocity field after 30 iterations.

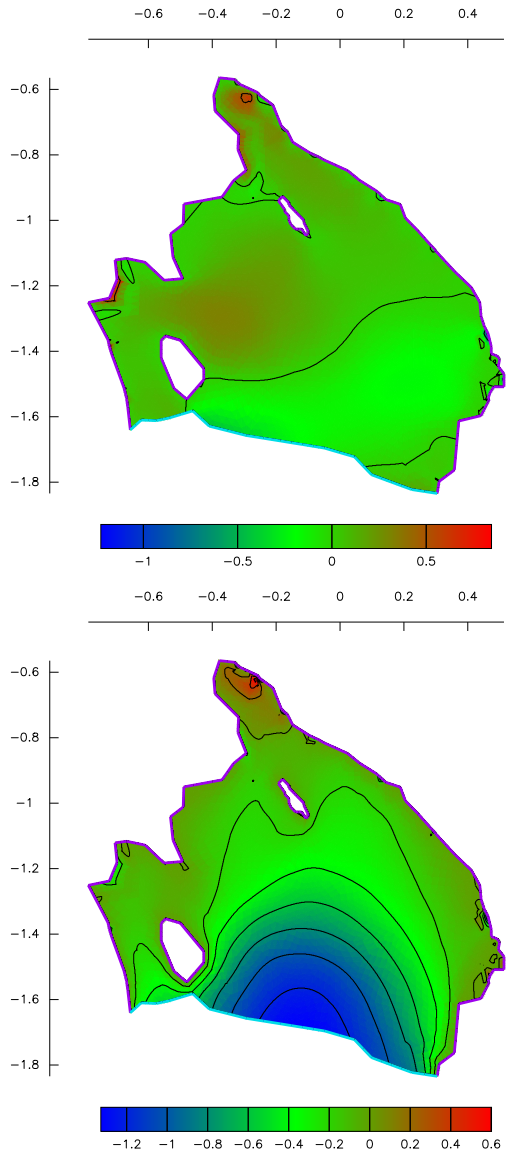

Figure II.31.: Computed v_x and v_y velocity components.

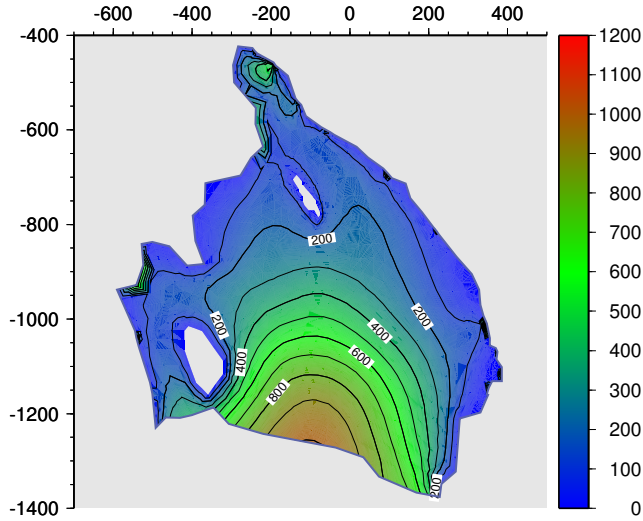

(a) Computed velocities in $\mathrm{m\,a^{-1}}$.

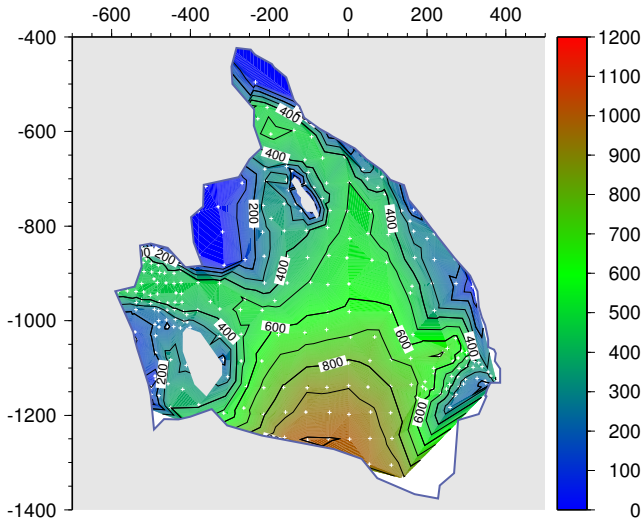

(b) Composed NSIDC velocity data. White crosses indicate measurement positions.

Figure II.32.: Comparison of computed and measured velocity data.

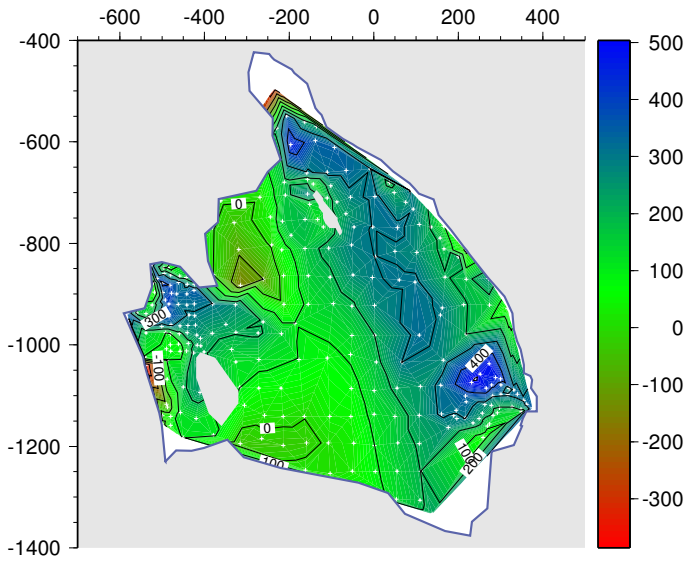

(a) Difference between computed and measured velocities, evaluated at the white crosses.

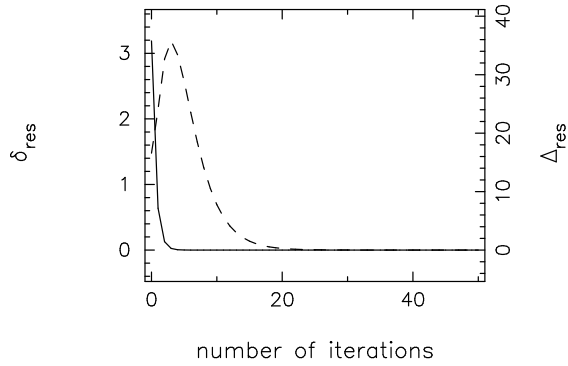

(b) δ_{res} (solid) and $\triangle_{\text{res}}$ (dashed) for the computation of the Ross Ice Shelf.

Figure II.33.: Results from the computation for the Ross Ice Shelf

Outlook

The theoretical model as well as the implementation of the finite element formulation can be used as a basis for further research. As far as the theory is concerned, there are two major topics where further research is sensible. First of all, the transition zone between the inland ice sheet and the ice shelf is not well understood yet. The main reason for this is that the zeroth order equations derived for either side of the grounding line do have a completely different mathematical structure. Even though Baral (2000) derives further approximations up to the second order for both, the ice-sheet as well as the ice-shelf equations, it is still not clear if and how both approximations can be matched together across the grounding line. Unfortunately, the second order equations derived are far more complicated than the zeroth order approximations already are. Since this holds at least for ice shelves, it is presently not foreseeable if these higher order equations will ever be implemented numerically. On the other hand, presumed that the present advance in computer technology and in the development of new, efficient numerical algorithms continues, it is likely that someone will solve the full 3D Stokes flow equations without any need for certain approximations in the future. Such a model could be applied to both, ice sheets as well as ice shelves, and it also holds along the transition zone. Even if such a model existed, it would not immediately solve all the questions that could be asked, since the dynamics of ice shelves is influenced by many processes that do have very different time scales. For example, the position of the grounding line changes by several meters twice a day due to tidal motion. The influence of these changes on the long term ice-shelf flow behaviour is just one issue that cannot be addressed by even the smartest 3D model as long as it describes the ice as a viscous fluid. Another issue of great relevance is the break-off of huge ice bergs from several ice shelves during the last years. It is likely that at least some of the mechanisms responsible for these events occur on shorter time scales, for example a weakening of

the ice structure due to crevasses that are created from surface melting is discussed.

The other, mostly unsolved topic is the calving process. Here, an extended version of the numerical model that solves the evolution equation for the ice thickness as well as that for the calving front would permit the test of a different parametrisations for the calving rate. Surely, the numerical model could also be extended to include some more of the processes that are only described theoretically at this stage. Good candidates to start with are the temperature and the ice-thickness evolution equations. Once all this is implemented, the marine ice layer could be added.

A. Stereographic projection

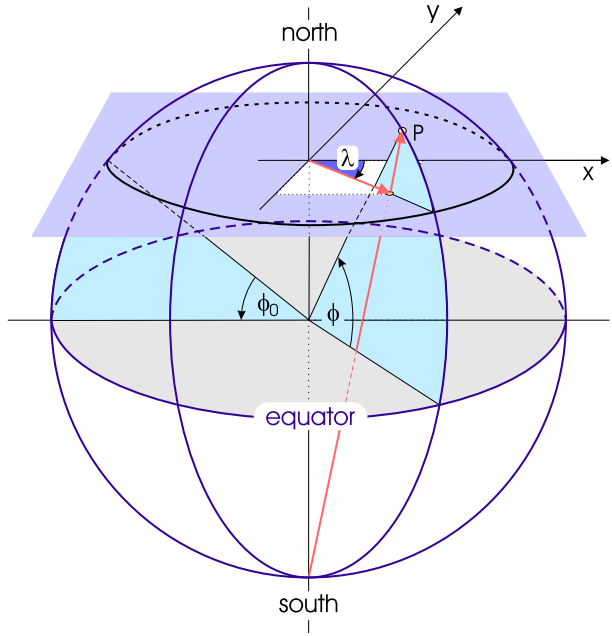

Figure A.1.: Stereographic projection.

One of the most commonly used projections to map polar regions onto a plane is the *stereographic projection*. It is defined by cutting the a sphere with an infinite plane at an arbitrarily chosen latitude*; the projected positions of points on the sphere onto this plane are the intersections of rays originating from a pole. This way, all points on the sphere except

*Commonly, 71°North is chosen.

the pole of projection (singularity) are mapped onto the plane (fig. A.1 illustrates the mapping procedure).

This way, a conformal mapping is defined. Mathematically, the projection of a point on the sphere with latitude ϕ and longitude λ to a Cartesian coordinate system in the plane with components x and y is found to be

$$x = \mu \tan\left(\frac{\pi}{4} - \frac{\phi}{2}\right) \sin\left(\lambda - \lambda_0\right), \tag{A.1}$$

$$y = \mu \tan\left(\frac{\pi}{4} - \frac{\phi}{2}\right) \cos\left(\lambda - \lambda_0\right); \tag{A.2}$$

λ_0 adjusts the orientation of the Cartesian coordinate system in the plane, while μ is a constant stretching factor depending on the latitude of the cutting plane, ϕ_0, and the radius of the sphere R_e,

$$\mu := R_\mathrm{e}\left[1 + \cos\left(\frac{\pi}{2} - \phi_0\right)\right]. \tag{A.3}$$

The inverse mapping is given by

$$\lambda = \lambda_0 + \operatorname{atan}\frac{x}{y}, \tag{A.4}$$

$$\phi = \frac{\pi}{2} - 2\operatorname{atan}\frac{\sqrt{x^2 + y^2}}{\mu}. \tag{A.5}$$

Applying a stereographic projection to the Earth is more complicated due to the flattening that is observable at polar regions and which is caused by centrifugal forces. To account for these deviations from being a sphere, ellipsoids or geoids are used. For those geometries, however, the mapping equations depend on the actual description of the Earth, and there are many different ellipsoidals and geoids in use today.

Stereographic projections do not preserve distances in general; only the distance between two points with latitudes ϕ_0 is preserved. Depending on the position, deviations between the distance on the sphere and that in the plane of projection are more or less pronounced. Fig. A.2 shows the relative deviation of distances between adjacent points along a meridian above a plane at $\phi_0 = 71\,^\circ$North with $R_\mathrm{e} = 6.300\,\mathrm{km}$. It shows that the deviation remains less than a few percent for the northern polar region. Furthermore,

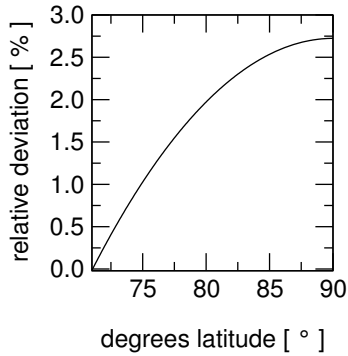

Figure A.2.: Deviation of distances in the stereographic plane relative to those on the sphere.

these deviations are upper limits to deviations that are expected from the mappings of ellipsoidal or geoidal coordinate systems of the Earth since those account for the Earth being "flatter than a sphere" in polar regions. This justifies deriving the ice-shelf equations for a Cartesian coordinate system in the plane of projection for a sphere rather than doing this in spherical or Earth (ellipsoidal of geoidal) coordinates.

B. Flow laws for ice

In order to obtain numerical results that are reliable and hold a comparison well with data obtained from field measurements, a thorough understanding of the flow properties of ice is crucial. Even though the continuum mechanical description of ice is well substantiated, determining the parameters involved is a very complicated task. This is not only because water, due to its dipole nature, is not a simple material, but also because ice behaves differently on different time scales. At the lower end of the time scales, the behaviour of ice can be modelled in terms of a linear elastic solid. Such a description is well suited, e.g. for acoustic-wave propagation in ice. This is likely to be the lower limit glaciologists are interested in, since the travel times of acoustic waves in ice are widely used to determine ice thicknesses as well as the internal structure of ice masses by seismic experiments. Often, however, one is interested in much larger time scales of at least several years. The upper limit of the times scales are several hundred thousand or even up to some million years when determining the long term behaviour of ice masses under changing climatic conditions. From these time scales alone, it should be clear that experiments performed in order to obtain material parameters for the fluid like behaviour of ice at such large time scales are very expensive and time consuming.
The following section discusses some of the major observations, as far as they are relevant for ice shelves. Much of it, including an extensive list of references, can be found in Paterson (1994).

Under natural pressure conditions, the water molecules arrange themselves in a hexagonal grid. A single crystal is composed of layers of hexagons*. The plane of the hexagons – in fact the molecules are arranged in two parallel planes with a certain distance from each other – is called the *basal plane* and the direction perpendicular to it the *c-axis*. Generally, such a single

*Ice possesses 12 different crystal structures and two amorphous states.

crystal is far from being perfect; there are many dislocations, which are linear defects, where individual layers are shifted against each other. A single crystal subjected to some stress field, e.g. uniaxial compression, immediately starts to deform along the dislocations. Even though the deformation of a crystal in other directions is possible as well, the displacement of layers along basal planes is dominant, since the stress needed is several hundred times less than that for a deformation in any other direction. Within the basal plane, there seems to be no preferred direction. Ice, therefore, is a strongly anisotropic material. Since the dislocations are transported while deforming the crystal, they may "pile up" at some stage resulting in a hardening of the material. Ice may also get softer again when the dislocations get more or less uniformly dispersed.

Typical creep curves for polycrystal ice – i.e. plotting strain versus time for a mixture of many individual crystals with random orientations – show up to five different flow behaviours. These range from a linear elastic behaviour to different kinds of creeping states. The *primary* or *transient creep* is characterized by continuously decreasing strain rates until a minimum is reached, the *secondary creep*; this minimum was observed for strains of 1 %, independent of the temperature and the stress. The minimum creep rate is less than 1 % of the steady creep rate of a single crystal along the basal plane. The strain rate increases again after that, this is called *tertiary creep*; it becomes steady after a total compressive strain of about $10 - 15\,\%$. Apart from the deformation of the individual crystals, there are several other mechanisms contributing to the overall deformation of polycrystalline ice: the single crystals are moving against each other, crystal growth and grain-boundary migration as well as dynamic recrystallisation may occur. The latter plays an important role for higher temperatures and starts at around $-12\,^{\circ}\mathrm{C}$. Microcracks may also be involved. The growth of individual crystals is inhibited by an increasing nucleation until some steady state is reached; this only depends on the stress field applied and not on the original grain sizes before the deformation started.

In the past, a wealth of research was done to estimate the material parameters from both, laboratory experiments as well as from observation of natural ice masses like glaciers, ice sheets and ice shelves. While laboratory experiments were restricted to simple stress fields like uniaxial compression and simple shear, the natural ice of glaciers, ice sheets or ice shelves is exposed to much more complicated stress fields that have to be estimated properly in order to obtain meaningful results from field measurements.

Typical field experiments are borehole tilting, i.e. the inclination of boreholes due to shear, as well as borehole or tunnel closure due to the pressure of the overlying ice. Furthermore, the spreading of ice shelves was used. All methods applied have their own specific problems. The major constraint of lab experiments simply is time. Most often only the minimum of the secondary creep can be reached, even though some experiments were performed over several years. During all this time, the external conditions like temperature had to be kept constant. The advantage of field measurements is that they do not have the time constraint and ice at nearly any interesting age can be found. There is, however, the problem of estimating the stress field which is not a simple task. Even though rough approximations like the assumption of simple shear are made, the situation is often complicated by longitudinal stresses that may play a dominant role especially in glacier flow. Often, a constant stress profile across a borehole has to be assumed for closure experiments, but this might not be an adequate description of the situation found in the field. In principle, the complete history of the probes has to be known due to its influence on the material properties.

Apart from these principle difficulties, there are many other effects that influence the flow properties like anisotropy or impurities. Dispersed particles like sand or ashes were found to potentially both harden or soften the ice depending on, e.g. the concentration of the particles. Even soluble impurities like HF, NH_3 and HCl effect the flow properties as they replace H_2O molecules in the grid; they generally weaken the ice. It was found from large boreholes in Greenland that the flow properties are different for ice from different periods: the secondary creep rate of Wisconsin or Würm ice is about 3.5 times that of Holocene ice. Many ice sheet models consider this by introducing an additional *enhancement factor* E in eq. (I.1.14). This weakening is explained by impurities like dust and enhanced chloride and sulphate concentrations, different grain sizes as well as anisotropy. A gas content in form of small bubbles seems not to have a significant influence. Of course, this is different for firn, which, however, is a totally different, compressible material.

Since all these effects may have to be taken into account when deriving flow parameters from measurements, it is quite understandable that measured strain rates for a given stress and temperature differ by a factor of ten, cf. Paterson (1994). In principle, there are two parameters that have to be determined from measurements for this power law, the rate factor

$A(T)$ and the exponent n. According to Paterson (1994), the exponent is found to be in the range $1.5 \leq n \leq 4$, but most commonly $n = 3$ is used; Hooke (1981) even cites values obtained from field data between 4 and 6. There are some observations showing n to increase for stresses larger than 5 bar, while it reaches a value near $n = 1$ – which describes a Newtonian fluid behaviour – for stresses lower that 1 bar.

The observation, that ice behaves more like a Newtonian fluid for very low stresses has also some relevance for the theoretical description of glacier and ice-sheet flow. As shown by Hutter (1983), several singularities occur whenever a power law rheology with $n > 1$ is used in combination with the SIA. These inconsistencies occur at locations where the SIA equations strictly do not hold, i.e. at the margins and at the ice divide. Such singularities can be avoided using what is called a *finite viscosity law* accounting for the Newtonian behaviour at low stresses by adding a constant term to the creep response function eq. (I.1.22).

T [°C]	$A(T)$ [kPa^{-3}s^{-1}]	method	reference
0	$93 \cdot 10^{-16}$	lab tests	Budd & Jacka (1989)
	$57 \cdot 10^{-16}$	tilting of 5 boreholes	Raymond (1980)
	$55 \cdot 10^{-16}$	closure of 2 tunnels	Nye (1953)
-2	$37 \cdot 10^{-16}$	lab tests	Steinemann (1958*a*), (1958*b*)
	$17 \cdot 10^{-16}$	lab tests	Barnes et al. (1971)
	$13 \cdot 10^{-16}$	lab tests	Morgan (1991)
	$27 \cdot 10^{-16}$	lab tests	Budd & Jacka (1989)
-10	$3.0 \cdot 10^{-16}$	lab tests	Shoji & Langway (1987)
	$3.5 \cdot 10^{-16}$	lab tests	Budd & Jacka (1989)
	$8.7 \cdot 10^{-16}$	borehole tilting	Dahl-Jensen & Gundestrup (1987)
	$5.3 \cdot 10^{-16}$	borehole closure	Thomas (1973*a*)
	$3.9 \cdot 10^{-16}$	ice-shelf spreading	Jezek et al. (1985)

Table B.1.: Measurements for the rate factor of Glen's flow law ($n = 3$), Paterson (1994).

Most often, the temperature dependence of the rate factor is described by an Arrhenius-type law as

$$A(T) = A_0 e^{-\frac{Q}{RT}}, \tag{B.1}$$

with a constant A_0, the absolute temperature T given in K, the universal gas constant $R = 8.314\,\mathrm{J\,mol^{-1}K^{-1}}$ and an activation energy Q. Since

RT is the thermal energy of the molecules within the crystal, this law can be motivated from the thermal energy that must be available in order for any molecule to move around within the lattice. Even though for a single crystal, the activation energy Q does not change with temperature, this is different for polycrystalline ice for which the activation energy increases as temperature approaches the melting point. It was suggested to explain the weakening of the material observed by grain boundary sliding due the presence of liquid water at the grain boundaries. It is common practice in ice modelling and it has been suggested in the EISMINT program to account for this fact by using two values of Q for two temperature ranges:

$$T < -10\,^{\circ}\mathrm{C} \;:\; Q = 60\,\mathrm{kJ\,mol^{-1}},$$

$$T \geq -10\,^{\circ}\mathrm{C} \;:\; Q = 139\,\mathrm{kJ\,mol^{-1}}.$$

Fig. B.1(a) shows some measurements cited in Paterson (1994) together with the two branches of eq. (B.1) for the two activation energies. A_0 is chosen for both branches to match a value of $A = 4.9 \cdot 10^{-16}\,\mathrm{kPa^{-3}\,s^{-1}}$ at $T = -10\,^{\circ}\mathrm{C}$,

$$T < -10\,^{\circ}\mathrm{C} \;:\; A_0 = 3.986 \cdot 10^{-4}\,\mathrm{kPa^{-3}\,s^{-1}},$$

$$T \geq -10\,^{\circ}\mathrm{C} \;:\; A_0 = 1.916 \cdot 10^{12}\,\mathrm{kPa^{-3}\,s^{-1}}.$$

Values for the rate-factor recommended by Paterson (1994) are summarized in table B.1(b). It should be stressed that in the temperature range between $-30\,^{\circ}\mathrm{C}$ and $0\,^{\circ}\mathrm{C}$, the rate factor varies over more than two orders of magnitude, i.e. the flow properties depend very strongly on temperature.

Superimposing some hydrostatic pressure on the stress field may result in a different material behaviour. To account for this, most often the homologous temperature T' is used in eq. (B.1) rather than the absolute temperature. This approach seems to go back to Rigsby (1958). Even though it is plausible that the activation energy may depend on the hydrostatic pressure applied, it is much harder to explain why one should use the homologous temperature. Rigsby's results were obtained by using a single crystal and most of the measurements where performed not far away from the pressure corrected melting point, well inside the range where recrystallisation would occur for polycrystalline ice. It is not clear whether

the results are transferable to polycrystalline ice. Hooke (1981) gives a somewhat different relation for the rate factor in terms of the absolute temperature,

$$A(T) = A_0 e^{-\frac{Q}{RT} + \frac{3C}{(T_\mathrm{r} - T)^k}}; \tag{B.2}$$

where $A_0 = 2.9477\,\mathrm{kPa^{-3}\,s^{-1}}$, $Q = 78.8\,\mathrm{kJ\,mol^{-1}}$, $T_\mathrm{r} = 273.39\,\mathrm{K}$, $C = 0.16612\,\mathrm{K}^k$ and $k = 1.17$. He obtained this relation as a fit to both, published laboratory data and field measurements. This parameterization is also shown in fig. B.1(a) as the dashed line. For the inverse relation, eq. (I.1.24), he gives the following relation

$$B(T) = B_0 e^{\frac{T_0}{T} - \frac{C}{(T_\mathrm{r} - T)^k}}, \tag{B.3}$$

with $B_0 = 6.984 \cdot 10^{-6}\,\mathrm{kPa\,s^{\frac{1}{3}}}$ and $T_0 = 3155\,\mathrm{K}$. Even though he considers the circumstances of how the measured values were obtained very carefully and estimates their quality, he found the scatter of the values to represent a variation of more than four in strain rate. For this reason, he concludes his paper with: "Put simply, it does not appear to be possible, at present, to estimate the velocity at a given point on a glacier to within a factor of at least 3 and perhaps higher."Results obtained from the more classical Arrhenius approach are of no better quality, and there seems to be no substantial improvement of this until today. One might argue that recent ice sheet and glacier models do a rather good job in calculating velocity fields and that they show a good agreement with measurements. However, those models generally do not depend only on the flow law but also on other parameters that are adjusted to achieve this good agreement. Furthermore, approximations like the SIA are often used and these do not hold over the complete ice sheet, and there are many more physical parameters like temperature, texture or the fabric of the ice that are hardly accessible for any global verification of model results; these quantities do have a large impact on the flow properties but measurements are only available at certain borehole locations. These critical remarks on the modelling of ice masses should, however, by no means derate the value of those calculations. Since one cannot simply "play around" with ice sheets and shelves, computer simulations are one very valuable tool to find out something about their dynamic behaviour. Nevertheless, one should always keep in mind the weak understanding of the material ice that is behind all these models. A good portion of scepticism is always advisable when analysing numerical results.

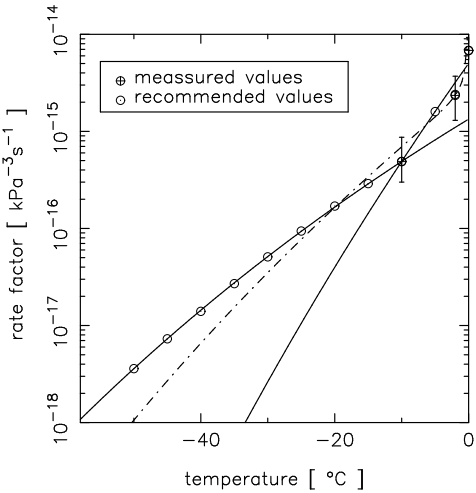

(a) Temperature dependence of the rate factor for Glen's flow law ($n = 3$). Further explanations in the main text.

T [°C]	$A(T)$ [kPa^{-3}s^{-1}]
0	$6.8 \cdot 10^{-15}$
-2	$2.4 \cdot 10^{-15}$
-5	$1.6 \cdot 10^{-15}$
-10	$4.9 \cdot 10^{-16}$
-15	$2.9 \cdot 10^{-16}$
-20	$1.7 \cdot 10^{-16}$
-25	$9.4 \cdot 10^{-17}$
-30	$5.1 \cdot 10^{-17}$
-35	$2.7 \cdot 10^{-17}$
-40	$1.4 \cdot 10^{-17}$
-45	$7.3 \cdot 10^{-18}$
-50	$3.6 \cdot 10^{-18}$

(b) Recommended values for the rate factor of Glen's flow law ($n = 3$) according to Paterson (1994).

Figure B.1.: Rate factor for Glen's flow law ($n = 3$).

Most ice sheet modellers seem to use eq. (B.1) together with the homologous temperature, but there are also authors who use eq. (B.2), e.g. Mangeney et al. (1996). As far as the ice-shelf problem is concerned, Hooke's equation has a large advantage since it does not depend on the homologous temperature. As seen from eq. (I.3.4), the longitudinal stress t_z^{D} contributes to the pressure distribution and therefore has to be known in order to calculate T'. This, however, introduces another coupling to the ice-shelf equations that would have to be handled somehow. No matter whether the pressure correction of the melting point actually influences the rate factor or not, either using Hooke's equations or just neglecting the influence of the pressure on the rate factor can be used to simplify the ice-shelf problem. Alternatively, the homologous temperature can be calculated from the geometry of the ice shelf only, neglecting the effect of the longitudinal stress t_z^{D} on the pressure distribution. Either approximation seems to be reasonable since the flow law is only precise to some factor anyhow.

The water content of marine ice may also have a significant effect on the flow properties of polycrystalline ice. According to Paterson (1994), the enhanced deformation can be explained by the water facilitating the adjustment between neighbouring grains with different orientations due to grain-boundary sliding and phase transitions. For the Arrhenius type equation, he gives the following relation between the A_0 and the water content w

$$A_0 = (3.2 + 5.8w) \cdot 10^{-15}\,\mathrm{kPa}^{-3}\,\mathrm{s}^{-1}. \tag{B.4}$$

It may turn out that it is necessary to account for this for the marine-ice layer.

C. Scaling of the vertical shear stresses

With the scalings of the stresses used in the main text, the vertical shear stresses t^{D}_{xz} and t^{D}_{yz} do not disappear from the local momentum balances in the SSA limit, eqs (I.2.4) – (I.2.6). However, if these stresses are assumed to be of even lower order in magnitude, e.g. $t^{\mathrm{D}}_{xz} = \mathcal{O}(\epsilon^2 \varrho\rho g[H])$ and $t^{\mathrm{D}}_{yz} = \mathcal{O}(\epsilon^2 \varrho\rho g[H])$, then

$$\text{(C.1)} \quad \frac{\mathcal{F}}{\varrho\epsilon}\frac{dv_x}{dt} = -\frac{\partial p}{\partial x} + \frac{\partial t^{\mathrm{D}}_x}{\partial x} + \frac{\partial t^{\mathrm{D}}_{xy}}{\partial y} + \epsilon\frac{\partial t^{\mathrm{D}}_{xz}}{\partial z},$$

$$\text{(C.2)} \quad \frac{\mathcal{F}}{\varrho\epsilon}\frac{dv_y}{dt} = \frac{\partial t^{\mathrm{D}}_{xy}}{\partial x} - \frac{\partial p}{\partial y} + \frac{\partial t^{\mathrm{D}}_y}{\partial y} + \epsilon\frac{\partial t^{\mathrm{D}}_{yz}}{\partial z},$$

$$\text{(C.3)} \quad \frac{\mathcal{F}}{\varrho}\epsilon\frac{dv_z}{dt} = \epsilon^3\frac{\partial t^{\mathrm{D}}_{xz}}{\partial x} + \epsilon^3\frac{\partial t^{\mathrm{D}}_{yz}}{\partial y} - \frac{\partial p}{\partial z} + \frac{\partial t^{\mathrm{D}}_z}{\partial z} - \frac{1}{\varrho}$$

and vertical shear stresses disappear in the SSA limit

$$\text{(C.4)} \quad -\frac{\partial p}{\partial x} + \frac{\partial t^{\mathrm{D}}_x}{\partial x} + \frac{\partial t^{\mathrm{D}}_{xy}}{\partial y} = 0,$$

$$\text{(C.5)} \quad \frac{\partial t^{\mathrm{D}}_{xy}}{\partial x} - \frac{\partial p}{\partial y} + \frac{\partial t^{\mathrm{D}}_y}{\partial y} = 0,$$

$$\text{(C.6)} \quad -\frac{\partial p}{\partial z} + \frac{\partial t^{\mathrm{D}}_z}{\partial z} = \frac{1}{\varrho}.$$

For this scaling of the stresses, the dual formulation of the stress-strain-rate relations becomes

$$t_x^{\mathrm{D}} = \frac{1}{\varrho}\mathcal{K}_{\mathrm{v}}\,\frac{1}{A(T)}\,g\left(d, A(T)\right)\,\frac{\partial v_x}{\partial x}, \tag{C.7}$$

$$t_y^{\mathrm{D}} = \frac{1}{\varrho}\mathcal{K}_{\mathrm{v}}\,\frac{1}{A(T)}\,g\left(d, A(T)\right)\,\frac{\partial v_y}{\partial y}, \tag{C.8}$$

$$t_z^{\mathrm{D}} = \frac{1}{\varrho}\mathcal{K}_{\mathrm{v}}\,\frac{1}{A(T)}\,g\left(d, A(T)\right)\,\frac{\partial v_z}{\partial z}, \tag{C.9}$$

$$t_{xy}^{\mathrm{D}} = \frac{1}{2\varrho}\mathcal{K}_{\mathrm{v}}\,\frac{1}{A(T)}\,g\left(d, A(T)\right)\left(\frac{\partial v_x}{\partial y} + \frac{\partial v_y}{\partial x}\right), \tag{C.10}$$

$$\epsilon^3 t_{xz}^{\mathrm{D}} = \frac{1}{2\varrho}\mathcal{K}_{\mathrm{v}}\,\frac{1}{A(T)}\,g\left(d, A(T)\right)\left(\frac{\partial v_x}{\partial z} + \epsilon^2\frac{\partial v_z}{\partial x}\right), \tag{C.11}$$

$$\epsilon^3 t_{yz}^{\mathrm{D}} = \frac{1}{2\varrho}\mathcal{K}_{\mathrm{v}}\,\frac{1}{A(T)}\,g\left(d, A(T)\right)\left(\frac{\partial v_y}{\partial z} + \epsilon^2\frac{\partial v_z}{\partial y}\right). \tag{C.12}$$

The pressure within the ice shelf given by eq. (I.3.8) is invariant to this re-scaling of the stresses and can be substituted into eqs (C.4) and (C.5). Therefore the re-scaled eqs (I.3.10) and (I.3.11) read in the SSA limit

$$2\frac{\partial t_x^{\mathrm{D}}}{\partial x} + \frac{\partial t_y^{\mathrm{D}}}{\partial x} + \frac{\partial t_{xy}^{\mathrm{D}}}{\partial y} = \frac{\partial H}{\partial x}, \tag{C.13}$$

$$\frac{\partial t_x^{\mathrm{D}}}{\partial y} + 2\frac{\partial t_y^{\mathrm{D}}}{\partial y} + \frac{\partial t_{xy}^{\mathrm{D}}}{\partial x} = \frac{\partial H}{\partial y}. \tag{C.14}$$

Substituting the stresses from eqs (C.7) – (C.10), this yields

(C.15)
$$\mathcal{K}_{\mathrm{v}}\left\{2\frac{\partial}{\partial x}\left[\frac{1}{A(T)}\,g\,(d,A(T))\;\frac{\partial v_x}{\partial x}\right]+\frac{\partial}{\partial x}\left[\frac{1}{A(T)}\,g\,(d,A(T))\;\frac{\partial v_y}{\partial x}\right]+\right.$$
$$\left.+\frac{\partial}{\partial y}\left[\frac{1}{A(T)}\,g\,(d,A(T))\;\frac{1}{2}\left(\frac{\partial v_x}{\partial y}+\frac{\partial v_y}{\partial x}\right)\right]\right\}=\varrho\,\frac{\partial H}{\partial x},$$

(C.16)
$$\mathcal{K}_{\mathrm{v}}\left\{\frac{\partial}{\partial y}\left[\frac{1}{A(T)}\,g\,(d,A(T))\;\frac{\partial v_x}{\partial x}\right]+2\frac{\partial}{\partial y}\left[\frac{1}{A(T)}\,g\,(d,A(T))\;\frac{\partial v_y}{\partial y}\right]+\right.$$
$$\left.+\frac{\partial}{\partial x}\left[\frac{1}{A(T)}\,g\,(d,A(T))\;\frac{1}{2}\left(\frac{\partial v_x}{\partial y}+\frac{\partial v_y}{\partial x}\right)\right]\right\}=\varrho\,\frac{\partial H}{\partial y}.$$

The terms on the right side depend only on the horizontal coordinates x and y. This is also true for the terms on the left hand side except those that depend on the temperature T. This, however, means that for vertically nonuniform temperature profiles – this is what is observed with the ice-shelf surface being some ten degrees below zero and the ice-shelf base being at $-2^{\circ}\mathrm{C}$ – different velocities are obtained from eqs (C.15) and (C.16) depending on the vertical position where the expressions containing T are evaluated. On the other hand, according to eq. (I.2.19) the horizontal velocities are vertically uniform. This means that the equations derived above are only consistent for a vertically uniform rate factor and are therefore not suitable to describe real ice shelves.

If, on the other hand, the scaling is performed as described in the main text, this inconsistency does not arise, since eqs (I.3.10) and (I.3.11) contain the vertical shear stresses even in the SSA limit. These stresses cannot be obtained from the zeroth order approximation of the stress-strain-rate relations, eqs. (I.2.27) and (I.2.28), but they are eliminated by vertical integration and applying the boundary conditions. Therefore, the consistency of the above equations does not arise. Since the vertical shear stresses are only present in the local formulation of the momentum balance, eqs (I.3.10) and (I.3.11), and furthermore, equations derived while neglecting them only hold for a thermomechanically decoupled modelling, i.e., ice shelves with a vertically uniform rate factor, these stresses can be interpreted as thermally induced stresses.

In spite of all these problems, equations similar to eqs (C.15) and (C.16) have been used in ice-shelf modelling, e.g. by Herterich (1990) and Determann (1991), and they are still used today. These equations can be obtained from the more generally valid eqs (I.3.28) and (I.3.29) by assuming a vertically constant rate factor, but it might be hard to guess the equations the other way around. A proper scaling analysis, however, leads – without any ad hoc assumptions – to the thermodynamically consistent eqs (I.3.28) and (I.3.29).

Notation

Bibliography

Babůska, I. & Aziz, A. (1976), 'On the angle condition in the finite element method.', *SIAM Journal of Numerical Analysis* **13**(2), 214–226.

Bamber, J. & Bentley, C. (1994), 'A comparison of satellite-altimetry and ice-thickness measurements of the Ross Ice Shelf, Antarctica', *Annals of Glaciology* **20**, 357–364.

Baral, D. (2000), Asymptotic theories of large scale motion, temperature and moisture distributions in land based polythermal ice shields and in floating ice shelves, PhD thesis, Institute of Mechanics, Darmstadt University of Technology, Darmstadt, Germany.

Baral, D., Hutter, K. & Greve, R. (2001), 'Asymptotic theories of large scale motion, temperature and moisture distributions in land based polythermal ice shields. A critical review and new developments', *Applied Mechanics Reviews, in press.*

Barnes, P., Tabor, D. & Walker, J. (1971), 'The friction and creep of polycrystalline ice', *Proc. R. Soc. London, Ser. A* **324**, 127–155.

BAS (1993), 1 edn, 'Antarctica – a topographic database', Sheet BAS (Misc) 7.

Bathe, K.-J. (1996), *Finite Element Procedures*, Prentice Hall.

Becker, E. & Bürger, W. (1975), *Kontinuumsmechanik*, B.G. Teubner, Stuttgart.

'BEDMAP Consortium' (2000), 'A new ice thickness and subglacial topographic model of the Antarctic', http://www.nerc-bas.ac.uk/public/aedc/bedmap/.

Bern, M. W. & Eppstein, D. (1995), Mesh generation and optimal triangulation, *in* D.-Z. Du & F. K.-M. Hwang, eds, 'Computing in Euclidean Geometry', second edn, number 4 *in* 'Lecture Notes Series on Computing', World Scientific, pp. 47–123.

Bindschadler, R., Vornberger, P., Blankenship, D., Scambos, T. & Jacobel, R. (1996), 'Surface velocity and mass balance of the Ice Streams D and E, West Antarctica', *Journal of Glaciology* **42**(142), 461–475.

Braess, D. (1997), *Finite Elemente*, Springer Verlag.

Braess, H. & Wriggers, P. (1998), 'Arbitrary Lagrangian Eulerian Finite Element Analysis of Free Surfaces Flow', *in press*.

Braithwaite, R. & Olesen, O. (1989), Calculation of glacier ablation from air temperature, West Greenland, *in* J. Oerlemans, ed., 'Glacier fluctuations and climatic change', Kluwer Academic Publishers, pp. 219–233.

Budd, W. (1969), 'The dynamics of ice masses', *ANARE Scientific Reports, Ser. A(IV), Glaciology*.

Budd, W. & Jacka, T. (1989), 'A review of ice rheology for ice sheet modelling', *Cold Regions Science and Technology* **16**, 107–144.

Calov, R. (1994), Das thermomechanische Verhalten des Grönländischen Eisschildes unter der Wirkung verschiedener Klimaszenarien - Antworten eines theoretisch-numerischen Modells, PhD thesis, Institut für Mechanik, Technische Universität Darmstadt, Germany.

Calov, R. (1998), 'A three-dimensional thermomechanical ice sheet model coupled to a climate model - theory, model test and application to the northern hemisphere ice sheets', Université Catholique de Louvain, Institute d'Astronomie et de Géophysique, Chemin du Cyclotron 2, B-1348 Louvain-la-Neuve.

Calov, R. & Marsiat, I. (1998), 'Simulations of the Northern Hemisphere through the last glacial-interglacial cycle with a vertically integrated and a three-dimensional thermomechanical ice sheet model coupled to a climate model', **27**, 169–176.

Chadwick, P. (1999), *Continuum Mechanics: Concise Theory and Problems*, 2 edn, Dover Publications.

Clausen, H., Dansgaard, W. & Nielsen, J. (1979), 'Surface accumulation on Ross Ice Shelf', *Antarctic Journal of the United States* **14(5)**, 68–72.

Dahl-Jensen, D. & Gundestrup, N. (1987), 'Constitutive properties of ice at Dye 3, Greenland', *IAHS* **170**, 31–43.

Determann, J. (1991), *Das Fließen von Schelfeisen - numerische Simulation mit der Methode der finiten Differenzen*, Vol. 83 of *Reports of Polar Research*, Alfred Wegner Institut für Polar- und Meeresforschung, Bremerhaven, Germany.

Duboius-Pélerin, Y. & Zimmermann, T. (1993), 'Object-orientated finite element programming: III. An efficient implementation in C++', *Computer Methods in Applied Mechanics and Engeneering* **108**, 165–183.

Engelhard, H. & Determann, J. (1987), 'Borehole evidence for a thick layer of basal ice in the central Rønne Ice Shelf', *Nature* **327**, 318–319.

Gammelsrød, T. & Slotsvik, N. (1981), 'Hydrographic and Current Measurements in the Southern Weddell Sea 1979/80', *Polarforschung* **51**(1), 101–111.

Gerland, S., Oerter, H., Kipfstuhl, J., Wilhelms, F. & Frenzel, A. (1996), Continuous Density Measurements of the Ice Core B25 from Berkner Island, Antarctica, *in* 'Filchner-Rønne Ice Shelf Programme (FRISP), Report **(10)**', Alfred-Wegener-Institut für Polar- und Meeresforschung, Bremerhaven, pp. 23–24.

Greve, R. (1995), *Thermomechanisches Verhalten polythermer Eisschilde – Theorie, Analytik, Numerik*, Berichte aus der Geowissenschaft, Shaker Verlag, Aachen, Germany.

Greve, R. (1997), 'A continuum-mechanical formulation for shallow polythermal ice sheets', *Philosophical Transactions Royal Society London, Ser. A* **355**, 921–974.

Greve, R. (2000), 'Waxing and Waning of the Perennial North Polar H_2O Ice Cap of Mars over Obliquity Cycles', *Icarus* **144**, 419–431.

Grosfeld, K. (1993), *Untersuchungen zu Temperaturregime und Massenhaushalt des Filchner-Rønne-Schelfeises, Antarktis, unter besonderer*

Berücksichtigung von Anfrier- und Abschmelzprozessen, Vol. 130 of *Reports of Polar Research*, Alfred Wegner Institut für Polar- und Meeresforschung, Bremerhaven, Germany.

Hansson, B. & Hooke, R. L. (2000), 'Glacier calving: a numerical model of forces in the calving-speed/water-depth relation', *Journal of Glaciology* **46**, 188–196.

Herterich, K. (1988), 'A three-dimensional model of the Antarctic ice sheet', *Annals of Glaciology* **11**, 32–35.

Herterich, K. (1990), *Modellierung eiszeitlicher Klimaschwankungen*, Habilitation thesis, Fachbereich Geowissenschaften, Universität Hamburg, Germany.

Hooke, R. (1981), 'Flow Law for Polycrystalline Ice in Glaciers: Comparison of Therretical Predictions, Laboratory Data, and Field Measurements', *Reviews of Geophysics and Space Physics* **19**(4), 664–672.

Hutter, J. & Williams, F. (1980), Theory of floating ice sheets, *in* P. Tryde, ed., 'Physics and mechanics of Ice', IUTAM Symposium Copenhagen 1979, Springer Berlin–Heidelberg–New York, pp. 145–162.

Hutter, K. (1983), *Theoretical Glaciology, Material Science of Ice and Mechanics of Glaciers and Ice Sheets*, D. Reidel Publishing Company, Terra Scientific Publishing Company; Dordrecht, Holland.

Huybrechts, P. (1992), *The Antarctic Ice Sheet and environmental change: a three-dimensional modelling study*, Vol. 99 of *Reports of Polar Research*, Alfred Wegner Institut für Polar- und Meeresforschung, Bremerhaven, Germany.

Huybrechts, P. (1993), 'Glaciological Modelling of the late cenozoic East Antarctic ice sheet: Stability or dynamism?', *Geografiska Annaler* **75A**, 221–237.

Jezek, K., Alley, R. & Thomas, R. (1985), 'Rheology of glacier ice', *Science* **227**, 1335–1337.

Liu, H., Jezek, K. & Li, B. (2000), 'Radarsat Antarctic Mapping Project Digital Elevation Model', http://nsidc.org/NASA/GUIDE/docs/dataset_documents/

radarsat_antarctic_mapping_project_digital_elevation_model_dataset_document.html.

MacAyeal, D. & Thomas, R. (1982), 'Numerical modeling of ice-shelf motion', *Annals of Glaciology* **3**(116), 189–194.

MacAyeal, D. & Thomas, R. (1986), 'The effects of basal melting on the present flow of the Ross Ice Shelf, Antactica', *Journal of Glaciology* **32**, 72–86.

MacAyeal, D., Rommelaere, V., Huybrechts, P., Hulbe, C., Determann, J. & Ritz, C. (1996), 'An ice-shelf model test based on the Ross Ice Shelf, Antarctica', *Annals of Glaciology* **23**, 46–51.

Mangeney, A., Califano, F. & Castelnau, O. (1996), 'Isothermal flow of an anisotropic ice sheet in the vicinity of an ice devide', *Journal of Geophysical Research* **101(28)**, 189/28,204.

Müller, I. (1973), *Thermodynamik*, Bertelsmann Universitätsverlag, Germany.

Morgan, V. (1991), 'High-temperature ice creep tests', *Cold Regions Science and Technology* **19**, 295–300.

Morland, L. (1984), 'Thermo-mechanical balances of ice sheet flows', *Journal of Geophysical and Astrophysical Fluid Dynamics* **29**, 237–266.

Morland, L. (1987), Unconfined ice-shelf flow, *in* C. Van der Veen & J. Oerlemans, eds, 'Dynamics of the West Antarctic Ice Sheet', D. Reidel Publishing Company, Terra Scientific Publishing Company; Dordrecht, Holland, pp. 99–116.

Nereson, N. (1998), The Flow History of Siple Dome and Ice Streams C and D, West Antarctica: Inferences from Geophysical Measurements and Ice Flow Models., PhD thesis, University of Washington.

Nye, J. (1953), 'The flow law of ice from measurements in glacier tunnels, laboratory experiments and the Junfraufirn borehole experiment', *Proc. R. Soc., London, Ser. A* **239**, 113–133.

Oerter, H., Kipfstuhl, J., Determann, J., Miller, H., Wagenbacht, D., Minikin, A. & Graf, W. (1992), 'Evidence for basal marine ice in the Filchner-Rønne ice shelf', *Nature* **358**, 399–402.

Ohmura, A. (1987), 'New temperature distribution map for Greenland', *Zeitschrift für Gletscherkunde und Glazialgeologie* **23**(1), 1–45.

Paterson, W. (1994), *The Physics of glaciers*, third edn, Pergamon Press, Oxford.

Raymond, C. (1980), Valley glaciers, *in* S. Colbeck, ed., 'Dynamics of Snow and Ice Masses', Academic Press, New-York, pp. 79–139.

Reddy, J. (1993), *An Introduction to the Finite Element Method*, 2 edn, McGraw-Hill Book Company.

Reeh, N. (1991), 'Parametrisation of melt rate and surface temperature in the Greenland ice sheet', *Polarforschung* **59**(3), 113–128.

Ridley, J. (1993), 'Surface melting on Antarctic Peninsula ice shelves detected by passive microwave sensors', *Geophysical Research Letters* **20**(23), 2639–2642.

Rigsby, G. (1958), 'Effect of hydrostatic pressure on velocity of shear deformed ice.', *Journal of Glaciology* **3**, 273–278.

Robin, G. (1975), 'Ice shelves and ice flow', *Nature* **253**, 168–173.

Sanderson, T. (1979), 'Equilibrium profile of ice shelves', *Journal of Glaciology* **24**(90), 435–459.

Scambos, T. A., Hulbe, C., Fahnestock, M. & Bohlander, J. (2000), 'The link between climate warming and break-up of ice shelves in the Antarctic Peninsula', *Journal of Glaciology* **46**, 516–530.

Scambos, T., Dutkiewicz, M., Wilson, J. & Bindschadler, R. (1992), 'Application of image cross-correlation to the measurement of glacier velocity using satellite image data.', *Remote Sensing Environ.* **42(3)**, 177–186.

Schmitting, W. (2000), Das Traveling Salesman Problem: Anwendung und Heristische Nutzung von Voronoi-/Delauny Strukturen zur Lösung eutektischer, zweidimensionaler Traveling Salesman Probleme, PhD thesis, Wirtschaftswissenschaftliche Fakultät der Heinrich-Heine Universität Düsseldorf, available online http://www.ulb.uni-duesseldorf.de/de/wiwi/1999/schmitting.html.

Schwarz, H. (1991), *Methode der finiten Elemente*, Teubner Studienbücher Mathematik.

Shabtaie, S. & Bentley, C. (1987), 'West Antarctic ice streamns draining into the Ross ice shelf: Configuration and Mass Balance', *Journal of Geophysical Research* **92**(B2), 1311–1336.

Shabtaie, S. & Bentley, C. R. (1982), 'Tabular Icebergs: Implications form Geophysical Studies of ice shelves', *Journal of Glaciology* **28**(100), 413–430.

Shewchuk, J. R. (1996*a*), 'A Two-Dimensional Quality Mesh Generator and Delaunay Triangulator', *http://www.cs.cmu.edu/~quake/triangle.research.html*.

Shewchuk, J. R. (1996*b*), Robust Adaptive Floating-Point Geometric Predicates, *in* 'Proceedings of the Twelfth Annual Symposium on Computational Geometry', Association for Computing Machinery, pp. 141–150.

Shewchuk, J. R. (1996*c*), Triangle: Engineering a 2D Quality Mesh Generator and Delaunay Triangulator, *in* M. C. Lin & D. Manocha, eds, 'Applied Computational Geometry: Towards Geometric Engineering', Vol. 1148 of *Lecture Notes in Computer Science*, Springer-Verlag, pp. 203–222. From the First ACM Workshop on Applied Computational Geometry.

Shewchuk, J. R. (1997), 'Adaptive Precision Floating-Point Arithmetic and Fast Robust Geometric Predicates', *Discrete & Computational Geometry* **18**(3), 305–363.

Shoji, H. & Langway, C. (1987), 'Flow velocity profiles and accumulation rates from mechanical tests on ice core samples', *IAHS* **170**, 67–77.

Smith, A. (1986), 'Ice Rumples on Rønne Ice Shelf, Antarctica', *British Antarctic Survey Bulletin* **72**, 47–52.

Smith, W. H. F. & Wessel, P. (1990), 'Gridding with continuous curvature splines in tension', *Geophysics* **55**(3), 293–305.

Smith, W. H. F. & Wessel, P. (1991), 'Free software helps map and display data', *EOS Trans. Amer. Geophys. U.* **72**(41), 441,445–446.

Smith, W. H. F. & Wessel, P. (1995*a*), 'New version of the Generic Mapping Tools released', *EOS Trans. Amer. Geophys. U. electronic supplement, http://www.agu.org/eos_elec/95154e.html*.

Smith, W. H. F. & Wessel, P. (1995*b*), 'New version of the Generic Mapping Tools released', *EOS Trans. Amer. Geophys. U.* **76**(33), 329.

Smith, W. H. F. & Wessel, P. (1998), 'New, improved version of Generic Mapping Tools released', *EOS Trans. Amer. Geophys. U.* **79**(47), 579.

Steinemann, S. (1958*a*), 'Experimentelle Untersuchungen zur Plastizität von Eis', *Beitr. Geol. Schweiz, Geotech. Ser.* **10**, 1–72.

Steinemann, S. (1958*b*), 'Resultats experimentaux sur la dynamique de la glace et leurs correlations avec le mouvement et la petrographie des glaciers', *IASH* **47**, 184–198.

Stroustrup, B. (1992), *Die C++ Programmiersprache*, 2 edn, Addison-Wesley.

Stroustrup, B. (1997), *The C++ Programming Language*, 3 edn, Addison-Wesley.

Thomas, R. H. (1973*a*), 'The creep of ice shelves: interpretation and observed behaviour', *Journal of Glaciology* **12**(64), 55–70.

Thomas, R. H. (1973*b*), 'The creep of ice shelves: theory', *Journal of Glaciology* **12**(64), 45–53.

Thomas, R., MacAyeal, D., Eilers, D. & Gaylord, D. (1984), 'Glaciological studies on the Ross Ice Shelf, Antarctica, 1973-1978', *Antarctic Research Series* **42**(Paper 2), 21–53.

Thyssen, F. (1988), 'Special aspects of the central part of Filchner-Rønne Ice Shelf, Antarctica', *Annals of Glaciology* **11**, 173–179.

Van der Veen, C. (1999), *Fundamentals of Glacier Dynamics*, 1 edn, A.A. Balkema.

Weertman, J. (1957), 'Deformation of floating ice shelves', *Journal of Glaciology* **24**(21), 38–42.

Weis, M., Greve, R. & Hutter, K. (1999), 'Theory of Shallow Ice Shelves', *Continuum Mechanics and Thermodynamics* **11**, 11–50.

Weis, M., Hutter, K. & Calov, R. (1996), '250.000 years in history of the Greenland Ice Sheet', *Annals of Glaciology* **23**, 359–363.

Whillans, I. & Van der Veen, C. (1993), 'New and improved determinations of velocity of Ice Streams B and C, Antarctica', *Journal of Glaciology* **39**, 483–490.

Williams, F. & Hutter, K. (1983), 'Thermal Response of Unconfined Ice Shelves to Climatic Conditions', *Acta Mechanica* **48**, 131–146.

Zienkiewicz, O. & Taylor, R. (1994*a*), *The Finite Element Method: Basic Formulation and Linear Problems*, Vol. 1, 4 edn, McGraw-Hill Book Company.

Zienkiewicz, O. & Taylor, R. (1994*b*), *The Finite Element Method: Solid and Fluid Mechanics, Dynamics and Non-linearity*, Vol. 2, 4 edn, McGraw-Hill Book Company.

Curriculum Vitae

persönliche Daten:

Name:	Magnus Weis
Geburtsdatum:	17.04.1969
Geburtsort:	Offenbach / Main
Familienstand:	ledig
Adresse:	Pommernstraße 25,
	64839 Münster / Altheim
1975 – 1979	Grundschule in Münster
1979 – 1981	Förderstufe in Münster
1981 – 1988	Gymnasium in Dieburg
Juni 1988	Abitur
1988 – 1990	Zivildienst,
	Johanniter-Unfall-Hilfe, Dieburg
1990 - 1996	Studium der Physik an der
	Technischen Hochschule Darmstadt
Februar 1996	Diplom-Hauptprüfung in Physik
1996 – 2001	wissenschaftlicher Mitarbeiter
	am Institut für Mechanik
	bei Prof. Hutter

contact: magnusweis@web.de